Chapter 1

The Quantum Field Imaging Paradigm

Parallel Quantum Metrology and Inverse Source Reconstruction

This chapter establishes the **complete QFI paradigm** and introduces the **two-layer taxonomy** that organizes the entire book. The fundamental task is **framework definition**: distinguishing Quantum Field Metrology (QFM) from Quantum Field Imaging (QFI) and establishing the operator stack as the unifying architecture.
The QFI paradigm accomplishes: (1) rigorous definitions separating field measurement from source reconstruction, (2) the complete operator stack $S \xrightarrow{\mathcal{G}} F \xrightarrow{\mathcal{M}} D \xrightarrow{\mathcal{R}} \hat{S}$ as the organizing framework, (3) figures of merit Q_{FOM} (throughput) and $Q_{\text{IFOM}} = Q_{\text{FOM}} \times \Gamma_{\text{inv}} \times \Gamma_{\text{mm}}$ (imaging fidelity), and (4) the QFI Gate criterion for unambiguous system classification.

QFI Pipeline Position: $\boxed{S} \xrightarrow{\boxed{G}} \boxed{F} \xrightarrow{\boxed{M}} \boxed{D} \xrightarrow{\boxed{R}} \boxed{\hat{S}}$ *(Complete stack introduction)*

Abbreviated Terms

Abbreviation	Definition
QFI	Quantum Field Imaging
QFM	Quantum Field Metrology
Q-FOM	Quantum Figure of Merit (measurement throughput)
Q-IFOM	Quantum Imaging Figure of Merit (includes reconstruction)
Q-OTF	Quantum Optical Transfer Function
NV	Nitrogen-Vacancy (center in diamond)
ODMR	Optically Detected Magnetic Resonance
CCD	Charge-Coupled Device
PMT	Photomultiplier Tube
SNR	Signal-to-Noise Ratio
FOV	Field of View
NA	Numerical Aperture
TSV	Through-Silicon Via
IC	Integrated Circuit
FA	Failure Analysis
SQUID	Superconducting Quantum Interference Device
CRB	Cramer-Rao Bound
Γ_{inv}	Reconstruction Fidelity Factor
Γ_{mm}	Model-Mismatch Penalty

Table 1.1: Abbreviated terms used in this chapter.

Abstract

This chapter establishes Quantum Field Imaging (QFI) as a distinct discipline within quantum metrology—one that transcends parallel field measurement to encompass inverse

source reconstruction with uncertainty quantification. We introduce a rigorous two-layer framework: **Quantum Field Metrology (QFM)** produces calibrated field maps $F(\mathbf{r})$, while **Quantum Field Imaging (QFI)** infers hidden sources $\hat{S}(\mathbf{r})$ from those maps using physics-based forward models $\mathcal{G}$ and reconstruction operators $\mathcal{R}$. The complete QFI operator stack $S \xrightarrow{\mathcal{G}} F \xrightarrow{\mathcal{M}} D \xrightarrow{\mathcal{R}} \hat{S}$ provides the organizing framework for the entire book. The QFM Figure of Merit (Q_{FOM}) quantifies measurement throughput, while the new Imaging Figure of Merit ($Q_{\mathrm{IFOM}} = Q_{\mathrm{FOM}} \times \Gamma_{\mathrm{inv}} \times \Gamma_{\mathrm{mm}}$) incorporates reconstruction fidelity. We demonstrate why this distinction matters through the historical parallel with CCD imaging and address the throughput bottleneck in semiconductor metrology. Nitrogen-vacancy (NV) centers in diamond serve as the exemplar platform for QFI implementation, uniquely enabling multi-physics sensing (magnetic, thermal, strain, noise) at room temperature.

1.1 Introduction: Why This Chapter Matters

1.1.1 Historical Context: The Measurement Paradigm Shifts

The evolution of measurement science has been punctuated by transformative paradigm shifts—moments when not just sensitivity improved, but the fundamental nature of data acquisition changed. In astronomical photometry, the replacement of photomultiplier tubes (PMTs) with charge-coupled devices (CCDs) in the 1980s represents the canonical example. Before CCDs, measuring stellar brightness required pointing a telescope at each star sequentially, collecting photons one object at a time. A skilled observer might achieve one star per minute with 5% photometric precision.

The introduction of CCD imaging enabled simultaneous measurement of thousands of stars in a single exposure. But the revolution was not merely about measuring faster—it was about enabling *imaging*: reconstructing spatial structure, enabling quantitative digital photometry, correlating sources across wavelengths, and ultimately discovering phenomena like dark energy through precision cosmology that would have been impossible with serial measurement.

The CCD Lesson

The CCD revolution succeeded not because it measured starlight faster, but because it enabled **quantitative imaging**—the reconstruction of spatial information that revealed new physics. QFI aims to replicate this paradigm shift for quantum sensing, where the critical distinction is between measuring fields (QFM) and reconstructing sources (QFI).

Quantum sensing stands at an analogous inflection point. Current quantum metrology tools—scanning NV magnetometers, atomic force microscopes with quantum tips, single-ion probes—achieve extraordinary sensitivity but remain fundamentally serial devices. The emerging field of **Quantum Field Imaging (QFI)** aims to do for quantum sensing what CCDs did for photometry: enable not just parallel acquisition, but true *imaging*—the reconstruction of hidden sources from measured fields with quantified uncertainty.

1.1.2 Pain Points in Current Semiconductor Metrology

The semiconductor industry faces a critical inspection bottleneck that conventional tools cannot address:

- **Throughput limitation**: Scanning NV probes require ∼7 hours to map a 50×50 µm region at sub-micrometer resolution
- **No buried-layer access**: Conventional optical tools cannot image through silicon substrates; X-ray CT is slow and lacks field sensitivity

- **Single-physics measurement**: Existing tools measure one physical quantity (magnetic OR thermal OR strain), missing correlated signatures
- **No source inference**: Current tools produce field maps at best, not defect identification or current reconstruction
- **Destructive testing**: Many failure analysis techniques (cross-section SEM, FIB) destroy the sample
- **3D IC complexity**: Advanced packaging (2.5D/3D, TSVs, chiplets) creates inspection challenges no existing tool solves

These pain points are not incremental—they represent fundamental gaps between what the semiconductor industry needs and what current metrology provides. QFI addresses each of these through a combination of parallel quantum measurement, multi-physics correlation, and source reconstruction.

1.1.3 Chapter Objectives and Figures of Merit

This chapter introduces the theoretical foundation that addresses these pain points. The key figures of merit are:

Figure of Merit	Target	Significance
Q_{FOM} (measurement throughput)	$> 10^8$ s^{-1}	Enable production-scale failure analysis
Q_{IFOM} (imaging throughput)	$> 10^7$ s^{-1}	Complete imaging with reconstruction
Γ_{inv} (reconstruction fidelity)	> 0.85	Accurate source inference from field maps
Γ_{mm} (model-mismatch penalty)	> 0.90	Robust to calibration errors
Φ_{multi} (multi-physics factor)	2–5	Depth disambiguation, false positive reduction
$\eta_q/\eta_{\text{classical}}$ (sensitivity ratio)	10–1000	Detect weak signals (nA currents, mK heating)
N_{parallel} (parallel channels)	10^4–10^6	Wide-field imaging

Table 1.2: Key figures of merit introduced in this chapter with target values and significance.

1.2 The Two-Layer Framework: QFM versus QFI

What QFI is NOT

Before defining what Quantum Field Imaging *is*, we clarify what it is *not*:

- **Not just parallel sensing**: Collecting N independent measurements simultaneously is wide-field metrology, not imaging.
- **Not just higher throughput**: Faster data collection without source inference remains metrology.
- **Not just better sensitivity**: Quantum-enhanced SNR without reconstruction is quantum metrology, not quantum imaging.

- **Not just NV centers**: The framework applies to any quantum sensor platform; NV is the exemplar.

QFI requires a complete imaging stack: forward model + measurement + inverse reconstruction + uncertainty quantification.

1.2.1 The Fundamental Distinction: Definitions

We introduce a two-layer taxonomy that precisely delineates the boundary between measurement and imaging:

Definition 1.2.1 (Quantum Field Metrology (QFM))**.** A **Quantum Field Metrology (QFM)** system simultaneously measures a spatially-varying physical field $F(\mathbf{r})$ using an array of N quantum sensors, producing a calibrated field map with quantified measurement uncertainty $\sigma_F(\mathbf{r})$. The output is the field itself.

Definition 1.2.2 (Quantum Field Imaging (QFI))**.** A **Quantum Field Imaging (QFI)** system estimates hidden sources or structures $\hat{S}(\mathbf{r})$ from measured field maps $F(\mathbf{r})$ using physics-based forward models $\mathcal{G}$ and reconstruction operators $\mathcal{R}$, providing uncertainty quantification $\sigma_S(\mathbf{r})$ for the estimated source. The output is the inferred source with confidence bounds, not the field.

The relationship is hierarchical: **QFI requires QFM as its measurement layer**, but QFM alone does not constitute imaging. This mirrors the classical distinction between radiometry (measuring optical power) and imaging (reconstructing spatial scenes).

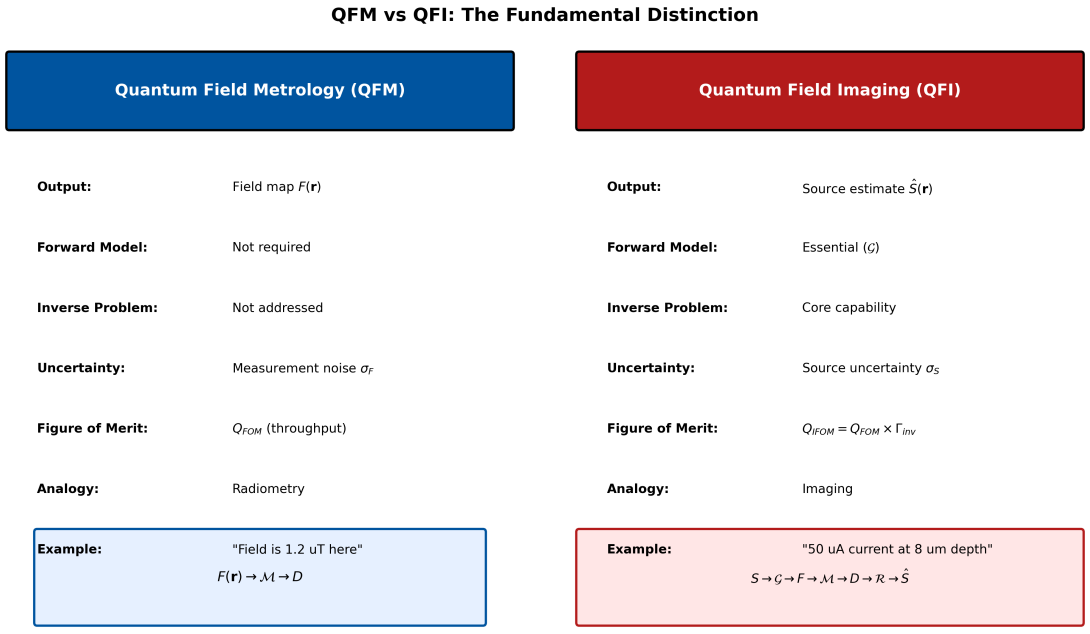

Figure 1.1: Visual comparison of Quantum Field Metrology (QFM) and Quantum Field Imaging (QFI). QFM produces calibrated field maps $F(\mathbf{r})$ as output, while QFI produces source estimates $\hat{S}(\mathbf{r})$ with uncertainty bounds through reconstruction. The operator stack shows the complete QFI pipeline extending beyond QFM.

Aspect	**QFM (Metrology)**	**QFI (Imaging)**
Primary output	Field map $F(\mathbf{r})$	Source estimate $\hat{S}(\mathbf{r})$
Forward model $\mathcal{G}$	Not required	Essential (physics operator)
Inverse problem	Not addressed	Core capability
Uncertainty output	Measurement noise σ_F	Source uncertainty σ_S
Validation metric	Calibration against known field	Reconstruction residual
Figure of merit	Q_{FOM} (throughput)	Q_{IFOM} (throughput × fidelity)
Classical analogy	Radiometry	Imaging
Example statement	"Field is 1.2 µT here"	"50 µA current at 8 µm depth"

Table 1.3: Systematic comparison of Quantum Field Metrology (QFM) and Quantum Field Imaging (QFI) across eight dimensions.

1.2.2 The Complete QFI Operator Stack

A QFI system implements the following operator chain, which serves as the organizing framework for this entire book:

The QFI Operator Stack

$$\boxed{S(\mathbf{r}) \xrightarrow{\mathcal{G}} F(\mathbf{r}) \xrightarrow{\mathcal{M}} D \xrightarrow{\mathcal{R}} \hat{S}(\mathbf{r}) \pm \sigma_S(\mathbf{r})} \tag{1.1}$$

where:

- $S(\mathbf{r})$: Hidden source distribution (e.g., 3D current density $\mathbf{J}(\mathbf{r})$, defect locations, material properties)
- $\mathcal{G}$: **Physics/Forward model operator** mapping source to field (e.g., Biot-Savart law for magnetic, thermal diffusion for temperature)
- $F(\mathbf{r})$: Physical field at sensor plane (e.g., magnetic field $\mathbf{B}(\mathbf{r})$, temperature $T(\mathbf{r})$)
- $\mathcal{M}$: **Measurement operator** (optics + quantum control + statistical estimator)
- D: Discrete measurement data (photon counts, ODMR spectra)
- $\mathcal{R}$: **Reconstruction/Inference operator** (inverse problem solver with regularization)
- $\hat{S}(\mathbf{r}) \pm \sigma_S(\mathbf{r})$: Estimated source with confidence bounds

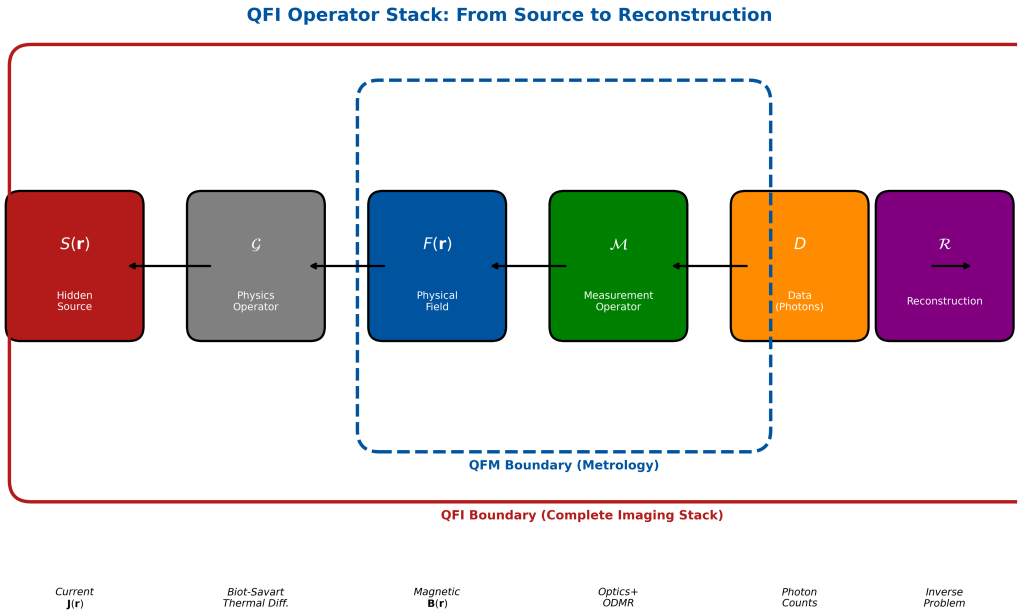

Figure 1.2: The complete QFI operator stack showing the transformation from hidden source $S(\mathbf{r})$ through forward model $\mathcal{G}$, measurement $\mathcal{M}$, and reconstruction $\mathcal{R}$ to estimated source $\hat{S}(\mathbf{r})$. The blue dashed boundary indicates the QFM layer (measurement only); the red solid boundary encompasses the complete QFI imaging stack. Each operator is developed in dedicated chapters of this book.

Design Rule 1.2.1: QFI Requires All Four Operators

A system qualifies as QFI only if it implements: (1) a validated forward model $\mathcal{G}$, (2) a quantum measurement system $\mathcal{M}$, (3) a reconstruction algorithm $\mathcal{R}$, and (4) uncertainty quantification for $\hat{S}$. Missing any component reduces the system to QFM.

1.2.3 The QFI Gate Criterion

To provide an unambiguous test for whether a system constitutes QFI, we define the **QFI Gate**:

The QFI Gate Criterion

If your deliverable is only $F(\mathbf{r})$, you are doing QFM.
You are doing QFI if and only if you deliver:

1. Source estimate $\hat{S}(\mathbf{r})$
2. Uncertainty bounds $\sigma_S(\mathbf{r})$
3. Reconstruction residual $\|D - \mathcal{M} \cdot \mathcal{G} \cdot \hat{S}\|$
4. Falsification test results (residual whiteness, etc.)

Missing ANY of these $\Rightarrow$ system is QFM, not QFI.

1.3 The Central Equations of Quantum Field Imaging

1.3.1 The QFM Figure of Merit (Measurement Throughput)

For the measurement layer, we define the throughput metric that quantifies how fast calibrated field data is acquired:

QFM Figure of Merit

$$\boxed{Q_{\text{FOM}} = \frac{\eta_q}{\eta_{\text{classical}}} \times \frac{N_{\text{parallel}}}{t_{\text{acquisition}}} \times \Phi_{\text{multi}}} \tag{1.2}$$

Units: s^{-1} (equivalent single-point classical measurements per second)

where:

- $\eta_q/\eta_{\text{classical}}$: **Quantum sensitivity advantage** (dimensionless, typically 10–1000×)
- $N_{\text{parallel}}/t_{\text{acquisition}}$: **Measurement rate** (pixels per second)
- Φ_{multi}: **Multi-physics correlation factor** (dimensionless, ≥ 1 when channels provide complementary information)

Critical insight: Q_{FOM} quantifies *how fast* we collect field data, not *how well* we recover source information. It is necessary but not sufficient for QFI performance.

1.3.2 The QFI Imaging Figure of Merit (Complete Imaging)

To capture the complete imaging capability including reconstruction quality, we introduce:

QFI Imaging Figure of Merit

$$\boxed{Q_{\text{IFOM}} = Q_{\text{FOM}} \times \Gamma_{\text{inv}} \times \Gamma_{\text{mm}}} \tag{1.3}$$

Units: s^{-1} (equivalent source-resolved measurements per second)

where:

- Γ_{inv}: **Reconstruction fidelity factor** ($0 < \Gamma_{\text{inv}} \leq 1$) — fraction of source variance successfully recovered, related to the Cramér-Rao bound
- Γ_{mm}: **Model-mismatch penalty** ($0 < \Gamma_{\text{mm}} \leq 1$) — accounts for forward model errors including PSF drift, standoff error, control field nonuniformity

Definition 1.3.1 (Reconstruction Fidelity Factor)**.** The reconstruction fidelity factor is defined as:

$$\Gamma_{\text{inv}} = \frac{\text{CRB}}{\text{MSE}_{\text{achieved}}} = \frac{\text{tr}(\mathbf{J}^{-1})}{\mathbb{E}[\|\hat{S} - S_{\text{true}}\|^2]} \tag{1.4}$$

where $\mathbf{J}$ is the Fisher Information matrix for source parameters.

Remark 1.3.1. $\Gamma_{\text{inv}} = 1$ indicates perfect source recovery (Cramér-Rao bound achieved); $\Gamma_{\text{inv}} \ll 1$ indicates that measurement noise or ill-conditioning prevents accurate source inference despite high Q_{FOM}. Typical values: $\Gamma_{\text{inv}} = 0.70$–$0.95$ for well-designed QFI systems.

1.3.3 Physical Interpretation of Each Factor

1.3.3.1 Factor 1: Quantum Sensitivity Advantage ($\eta_q/\eta_{\text{classical}}$)

The quantum sensitivity advantage arises from fundamental differences between quantum and classical sensing:

- **Shot-noise limited detection**: Quantum sensors operate at the photon shot-noise limit vs. thermal/Johnson noise in classical sensors
- **Quantum projection noise**: The fundamental measurement limit for spin systems scales as $1/\sqrt{N \cdot T_2}$
- **Coherent manipulation**: Pulse sequences enable optimized sensing protocols that classical sensors cannot implement

For NV centers measuring magnetic fields, the sensitivity is:

$$\eta_q \approx \frac{h \cdot \Delta\nu}{\gamma_e \cdot C \cdot \sqrt{R \cdot T_2^*}} \tag{1.5}$$

where $\gamma_e = 28$ GHz/T is the electron gyromagnetic ratio, C is the ODMR contrast ($\sim$0.03 for ensemble NV), R is the photon collection rate, and T_2^* is the inhomogeneous dephasing time.

Numerical benchmark: For typical NV parameters, $\eta_q \sim 1$ $\mu\text{T}/\sqrt{\text{Hz}}$ per NV center; for 10^6 NVs in parallel: ~ 1 $\text{nT}/\sqrt{\text{Hz}}$.

1.3.3.2 Factor 2: Parallelism ($N_{\text{parallel}}/t_{\text{acquisition}}$)

This factor captures the throughput advantage of wide-field acquisition over serial scanning:

System Configuration	N_{parallel}	**Throughput Impact**
Scanning NV probe	1	Baseline
128×128 pixel array	1.6×10^4	$10^4\times$ faster
512×512 pixel array	2.6×10^5	$10^5\times$ faster
1024×1024 pixel array	1.0×10^6	$10^6\times$ faster

Table 1.4: Parallelism factor for different array configurations, showing the dramatic throughput improvement from wide-field imaging.

1.3.3.3 Factor 3: Multi-Physics Correlation (Φ_{multi})

When measuring multiple correlated physical fields simultaneously, the total information exceeds the sum of individual measurements:

$$\Phi_{\text{multi}} = \frac{I_{\text{joint}}}{\sum_i I_{\text{individual}}} \geq 1 \tag{1.6}$$

A resistive defect in an IC creates correlated signatures across multiple physics channels:

- **Magnetic**: $B \propto I$ (Amperian current)
- **Thermal**: $T \propto I^2 R$ (Joule heating)
- **Strain**: From thermal expansion $\varepsilon \propto \alpha \Delta T$

Multi-physics measurement provides three critical benefits:

1. **Confirmation**: Reduces false positives by 10–100× through independent channel correlation
2. **Depth disambiguation**: Thermal diffusion has different spatial decay than magnetic field ($\sim 1/r^3$), enabling depth separation
3. **Physics insight**: Power $= I^2R$ enables resistance extraction from combined B and T measurements

Typical values: $\Phi_{\text{multi}} = 2$–5 for correlated IC defects.

1.3.3.4 Factor 4: Reconstruction Fidelity (Γ_{inv})

This factor—unique to QFI and absent in QFM—captures how well the inverse problem is solved:

Γ_{inv} **Range**	**Interpretation**	**Typical Scenario**
0.95–1.0	Excellent	Well-conditioned, high SNR, accurate forward model
0.85–0.95	Good	Typical multi-physics QFI with CAD priors
0.70–0.85	Moderate	Single-physics, moderate ill-conditioning
0.50–0.70	Poor	Severely ill-conditioned, regularization critical
< 0.50	Unacceptable	Redesign required; add physics channels

Table 1.5: Reconstruction fidelity factor interpretation guide.

1.3.3.5 Factor 5: Model-Mismatch Penalty (Γ_{mm})

Real systems deviate from ideal forward models. The model-mismatch penalty captures cumulative calibration errors:

$$\Gamma_{\text{mm}} = \prod_i (1 - \varepsilon_i^2) \approx 1 - \sum_i \varepsilon_i^2 \tag{1.7}$$

where ε_i are normalized error contributions:

Error Source	**Symbol**	**Typical** ε_i	**Mitigation**
Standoff distance error	$\varepsilon_{\text{standoff}}$	0.02–0.10	Autofocus, calibration
PSF spatial variation	ε_{PSF}	0.02–0.08	Field-dependent correction
Illumination nonuniformity	$\varepsilon_{\text{illum}}$	0.02–0.05	Flat-field calibration
MW field nonuniformity	ε_{MW}	0.03–0.10	Antenna optimization
Pixel response (PRNU)	$\varepsilon_{\text{PRNU}}$	0.01–0.03	Camera calibration
Diamond surface tilt	$\varepsilon_{\text{tilt}}$	0.01–0.05	Active leveling

Table 1.6: Model-mismatch penalty contributions and mitigation strategies.

1.3.4 The Multiplicative Principle

Design Rule 1.3.1: Target the Weakest Factor

System optimization should target the factor with lowest current performance, as improvements across all factors are **multiplicative**, not additive. For QFI systems, this often means prioritizing Γ_{inv} (reconstruction quality) over N_{parallel} (pixel count).

Improvement	QIFOM Impact
$10\times$ better quantum sensitivity	$10\times$
$100\times$ more pixels	$100\times$
Add second physics channel (Φ_{multi}: $1 \to 2$)	$2\times$
Improve Γ_{inv}: $0.70 \to 0.95$	$1.36\times$
Improve Γ_{mm}: $0.80 \to 0.95$	$1.19\times$
All combined	$\mathbf{3240}\times$

Table 1.7: Multiplicative impact of individual factor improvements on Q_{IFOM}.

1.4 Information-Theoretic Foundations

1.4.1 QFI as a Communication Channel

From an information-theoretic perspective, a QFI system is a communication channel—but critically, the relevant capacity is for *source parameters*, not field values.

QFI Channel Model

$$\text{Source } S \xrightarrow{\text{Physics } \mathcal{G}} \text{Field } F \xrightarrow{\text{Channel } \mathcal{M}} \text{Data } D \xrightarrow{\text{Decoder } \mathcal{R}} \text{Estimate } \hat{S} \tag{1.8}$$

The channel capacity for source recovery is:

$$I_{\text{QFI}} = \frac{1}{2} \log \det \left(\mathbf{I} + \mathbf{J}_S / \mathbf{J}_{\text{prior}} \right) \tag{1.9}$$

where $\mathbf{J}_S$ is the Fisher Information for source parameters and $\mathbf{J}_{\text{prior}}$ captures prior knowledge (e.g., from CAD files).

Remark 1.4.1. Unlike standard metrology where capacity scales simply with pixel count N, QFI capacity depends on the *conditioning* of the inverse problem. Adding pixels that provide redundant information (e.g., far from sources) yields diminishing returns. This is why Γ_{inv} appears explicitly in Q_{IFOM}.

1.4.2 Comparison: QFM vs QFI Information Content

Metric	QFM (Field)	QFI (Source)
Capacity scaling	$\propto N \cdot \log(1 + \text{SNR}_q)$	$\propto \log\det(\mathbf{I} + \mathbf{J}_S)$
Redundancy penalty	None (more pixels always helps)	Ill-conditioning reduces capacity
Multi-physics benefit	Additive (separate channels)	Multiplicative (rank increase)
Fundamental limit	Shot noise on field	Cramér-Rao bound on source

Table 1.8: Information-theoretic comparison of QFM and QFI.

1.4.3 Shot-Noise Limited SNR

For photon-counting measurements in the QFM layer:

$$\mathrm{SNR}_q = \sqrt{\eta_{\mathrm{opt}} \cdot P \cdot t/(h\nu)} \tag{1.10}$$

where η_{opt} is optical collection efficiency, P is collected power, t is integration time, and $h\nu$ is photon energy.

Design Rule 1.4.1: SNR Scaling with Integration Time

SNR scales as $\sqrt{t}$; doubling SNR requires 4× integration time. This makes parallelism (N_{parallel}) more efficient than longer integration for throughput improvement.

1.5 Throughput Analysis: Scanning vs. Wide-Field QFI

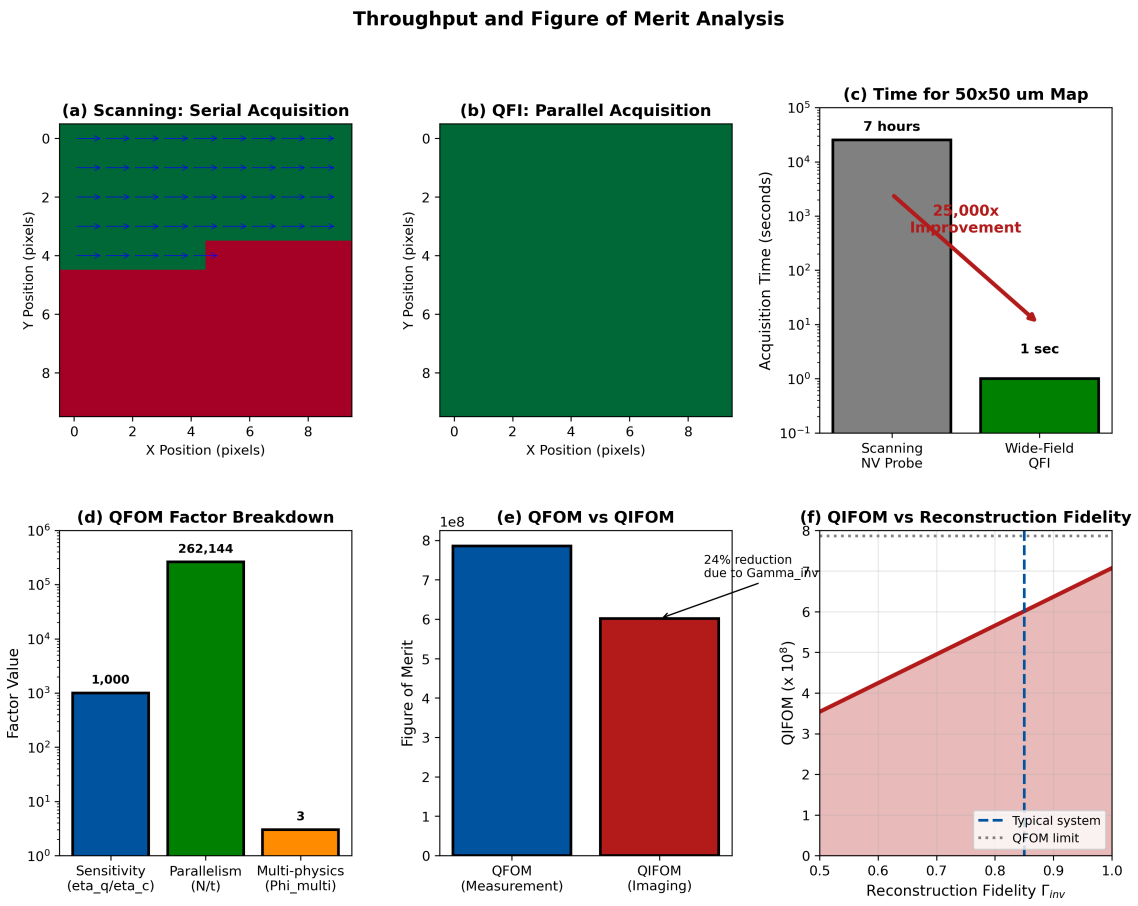

Figure 1.3: Comprehensive throughput and figure of merit analysis. (a) Scanning serial acquisition pattern. (b) QFI parallel acquisition—all pixels captured simultaneously. (c) Time comparison for 50×50 µm map: 7 hours (scanning) vs. 1 second (QFI), representing 25,000× improvement. (d) QFOM factor breakdown showing multiplicative contributions. (e) QFOM vs. QIFOM comparison revealing reconstruction impact. (f) QIFOM dependence on reconstruction fidelity Γ_{inv}.

1.5.1 Quantitative Throughput Comparison

Consider mapping a 50×50 µm region at 500 nm resolution (100 × 100 pixels):

Method A: Scanning NV Probe

- Dwell time per pixel: 100 ms (for adequate SNR)
- Total pixels: 10^4
- Total time: $10^4 \times 0.1$ s $= 1000$ s ≈ 17 minutes
- With overhead (positioning, feedback): $\sim$7 hours for realistic high-resolution scan

Method B: Wide-Field QFI

- All 10^4 pixels captured simultaneously
- Integration time for equivalent SNR: 1 second (with optimized diamond and high-NA collection)
- Throughput improvement: $\mathbf{25,000}\times$

1.5.2 QFOM Calculation Example

For a production QFI system with:

- Quantum sensitivity advantage: $\eta_q/\eta_{\text{classical}} = 1000$
- Parallel channels: $N_{\text{parallel}} = 512 \times 512 = 262,144$
- Acquisition time: $t_{\text{acquisition}} = 1$ s
- Multi-physics factor: $\Phi_{\text{multi}} = 3$ (B + T + strain)

$$Q_{\text{FOM}} = \frac{\eta_q}{\eta_{\text{classical}}} \times \frac{N_{\text{parallel}}}{t_{\text{acquisition}}} \times \Phi_{\text{multi}} \tag{1.11}$$

$$= 1000 \times 262,144 \times 3 \tag{1.12}$$

$$= 7.86 \times 10^8 \text{ s}^{-1} \tag{1.13}$$

1.5.3 QIFOM Calculation with Reconstruction

Adding reconstruction factors:

- Reconstruction fidelity: $\Gamma_{\text{inv}} = 0.85$ (typical multi-physics system)
- Model-mismatch penalty: $\Gamma_{\text{mm}} = 0.90$ (well-calibrated)

$$Q_{\text{IFOM}} = Q_{\text{FOM}} \times \Gamma_{\text{inv}} \times \Gamma_{\text{mm}} \tag{1.14}$$

$$= 7.86 \times 10^8 \times 0.85 \times 0.90 \tag{1.15}$$

$$= 6.01 \times 10^8 \text{ s}^{-1} \tag{1.16}$$

Interpretation: The 23% reduction from Q_{FOM} to Q_{IFOM} reflects reconstruction limitations. However, only Q_{IFOM} captures the true imaging capability—the throughput for delivering source estimates, not just field maps.

1.6 Multi-Physics Correlation Advantage

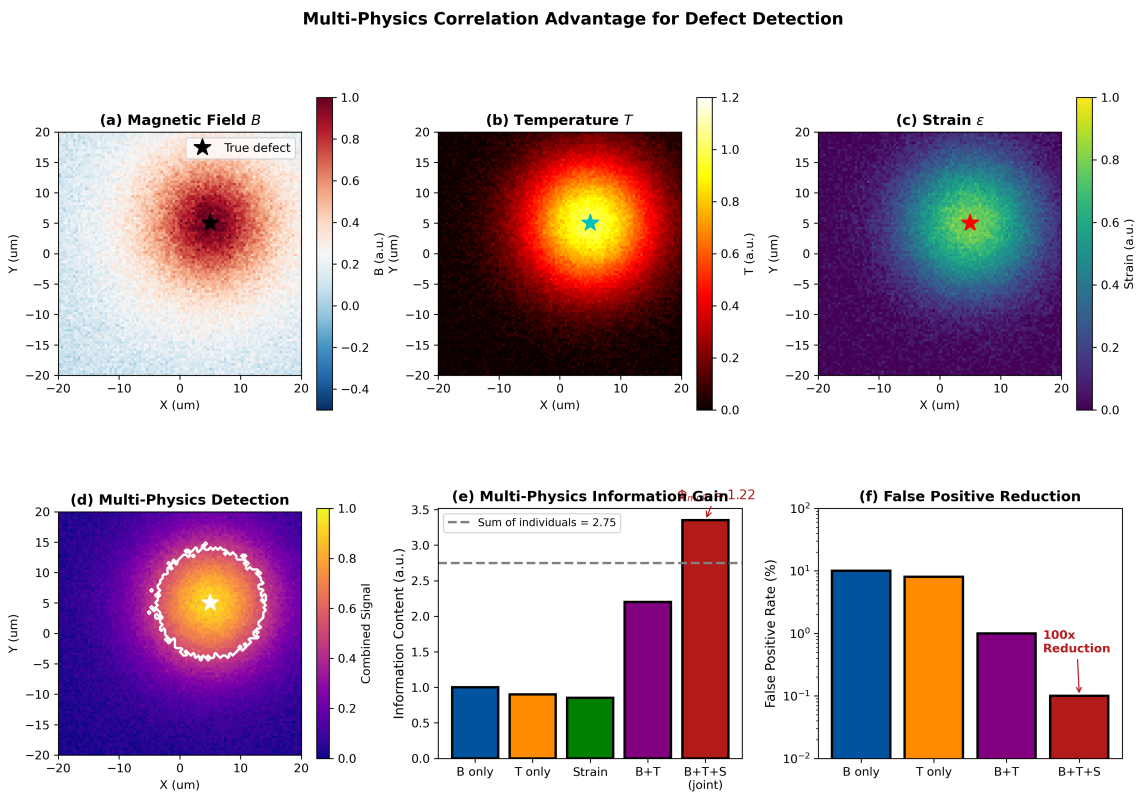

Figure 1.4: Multi-physics correlation advantage for defect detection. (a) Magnetic field channel showing dipole-like signature from current. (b) Temperature channel with broader diffusion pattern. (c) Strain channel from thermal expansion. (d) Combined multi-physics detection with improved localization. (e) Information gain analysis showing $\Phi_{\text{multi}} > 1$ for joint measurement. (f) False positive rate reduction: 100× improvement with B+T+Strain vs. single-physics.

1.6.1 Physical Basis for Multi-Physics Correlation

A buried defect (short circuit, resistive open, thermal hotspot) creates simultaneous signatures in multiple physical fields. Each channel has different spatial characteristics:

Channel	Source Dependence	Spatial Decay	Characteristic
Magnetic B	$\propto I$ (linear)	$\sim 1/r^2$ (dipole)	Sharp, localized
Thermal T	$\propto I^2 R$ (quadratic)	Diffusive (Gaussian)	Broad, diffused
Strain ε	$\propto \alpha \Delta T$	Follows T	Correlated with thermal

Table 1.9: Physical characteristics of multi-physics channels.

1.6.2 Depth Disambiguation through Multi-Physics

A critical challenge in QFI is the depth-amplitude ambiguity: a shallow weak source can produce the same magnetic signature as a deep strong source. Multi-physics measurement breaks this degeneracy because different channels have different depth dependencies:

- **Magnetic field**: Decays as $\sim 1/z^2$ (dipole) or $\sim 1/z^3$ (for extended sources)
- **Temperature**: Diffuses according to heat equation; characteristic width $\sim \sqrt{D \cdot t}$

- **Correlation**: Sharp magnetic + broad thermal ⇒ deep source

Design Rule 1.6.1: Multi-Physics Improves Both Φ_{multi} AND Γ_{inv}

Multi-physics measurement improves not just information content ($\Phi_{\text{multi}} > 1$) but also reconstruction fidelity (Γ_{inv}) by improving the conditioning of the inverse problem. The forward model matrix $\mathbf{G}_{\text{multi}}$ has higher rank than single-physics $\mathbf{G}_{\text{single}}$.

1.7 Historical Parallel: The CCD Revolution

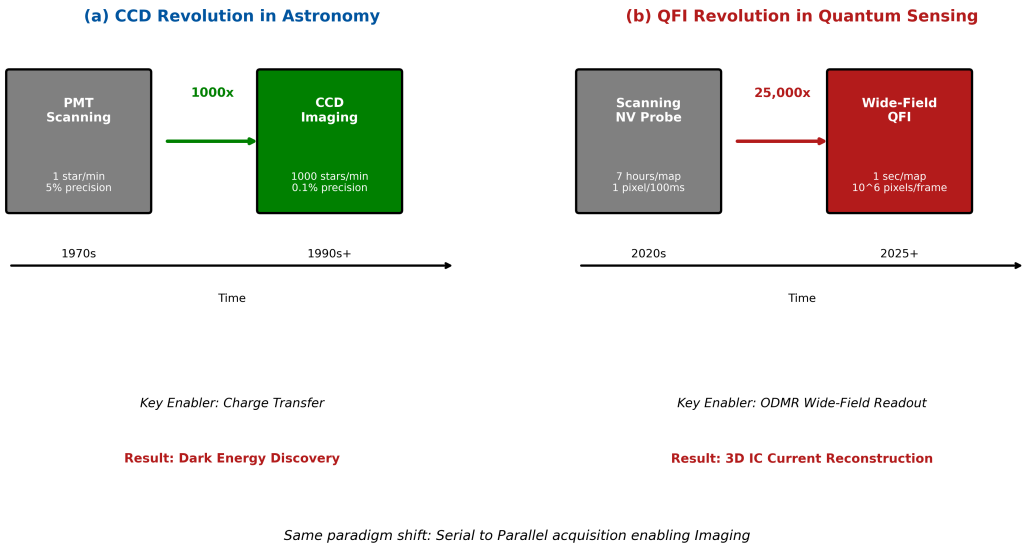

Figure 1.5: Historical parallel between the CCD revolution in astronomy and the QFI revolution in quantum sensing. Both transitions represent paradigm shifts from serial to parallel measurement that enabled true imaging, not just faster measurement. Key enablers were charge transfer (CCD) and ODMR wide-field readout (QFI). Scientific impact: CCD enabled dark energy discovery; QFI enables 3D IC source reconstruction.

1.7.1 Photometry Before CCDs

Before CCDs, astronomical photometry was dominated by PMT-based measurements:

- **Serial acquisition**: One star at a time, telescope repositioning between measurements
- **Throughput**: ∼1 star/minute with 5% photometric precision
- **Capability**: Brightness measurement only—no spatial reconstruction

1.7.2 The CCD Paradigm Shift

CCDs transformed astronomy not just through speed, but through *imaging*:

- **Parallel acquisition**: 10^6–10^9 pixels simultaneously
- **Throughput**: ∼1000 stars/minute with 0.1% precision
- **Capability**: Quantitative imaging enabling source characterization, astrometry, photometric redshifts

The crucial point: CCDs enabled the discovery of dark energy not because they measured supernova brightness faster, but because they enabled *precision imaging* that revealed subtle spatial correlations and standardizable candle light curves.

1.7.3 QFI as the Quantum Sensing CCD

Aspect	**Photometry (CCD)**	**Quantum Sensing (QFI)**
Serial method	PMT scanning	Scanning NV probe
Parallel method	CCD imaging	Wide-field QFI
Typical pixels	10^6–10^9	10^4–10^6 (current)
Key enabler	Charge transfer readout	ODMR wide-field readout
Throughput gain	1000–$10^6\times$	100–$10^6\times$
True innovation	Source characterization	**Source reconstruction**

Table 1.10: Exact parallel between CCD revolution and QFI paradigm shift.

Prediction: Just as CCDs revolutionized astronomy by enabling quantitative imaging that revealed dark energy, QFI will revolutionize semiconductor metrology by enabling source reconstruction that reveals buried defects invisible to field mapping alone.

1.8 Reconstruction Fidelity Analysis

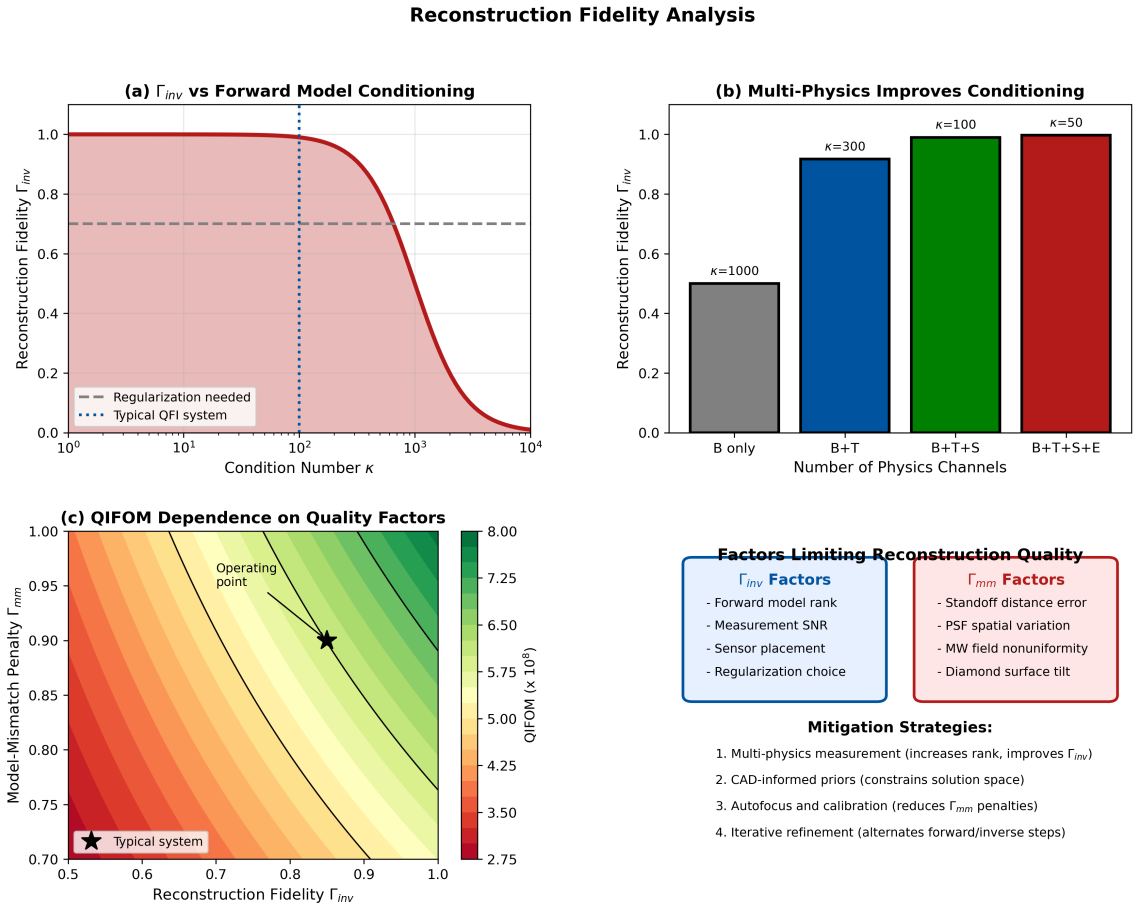

Figure 1.6: Reconstruction fidelity analysis. (a) Γ_{inv} dependence on forward model condition number κ, showing degradation for ill-conditioned problems. (b) Multi-physics improves conditioning: adding physics channels reduces κ and improves Γ_{inv}. (c) QIFOM surface as function of Γ_{inv} and Γ_{mm}, showing typical operating point. (d) Summary of factors limiting Γ_{inv} (forward model rank, SNR) and Γ_{mm} (calibration errors) with mitigation strategies.

1.8.1 The Inverse Problem Challenge

The transition from QFM to QFI requires solving an inverse problem: given measurements D, find source S such that $D \approx \mathcal{M} \cdot \mathcal{G} \cdot S$. This problem is typically ill-posed:

- **Non-uniqueness**: Multiple source configurations can produce identical field patterns (depth-amplitude ambiguity)
- **Ill-conditioning**: Small measurement noise amplifies to large source errors
- **Incompleteness**: 2D measurement of 3D source inherently loses information

1.8.2 Condition Number and Γ_{inv}

The reconstruction fidelity is fundamentally limited by the condition number κ of the discretized forward model:

$$\Gamma_{\text{inv}} \approx \frac{1}{1 + (\kappa/\kappa_0)^2/\text{SNR}^2} \tag{1.17}$$

where $\kappa_0 \sim 100$ is a reference condition number. This explains why:

- High SNR alone cannot save a poorly-conditioned problem
- Multi-physics improves Γ_{inv} by reducing effective κ
- CAD priors act as regularization, constraining the solution space

1.8.3 Design Proxy for Γ_{inv}

During system design (before ground-truth validation), use:

$$\Gamma_{\text{inv}}^{\text{proxy}} = \frac{1}{1 + \kappa/100} \tag{1.18}$$

This allows estimation of QIFOM during design without requiring experimental validation.

1.9 Taxonomy of QFI Systems

QFI Type	**Sensor**	**Primary Field**	**Platform**	Γ_{inv} **Potential**
Type I: Solid-state	NV, SiV centers	B, T, strain, E	Diamond arrays	High (0.85–0.95)
Type II: Atomic vapor	Rb, Cs atoms	B, RF	Vapor cells	Medium (0.70–0.90)
Type III: Superconducting	SQUIDs	B	Cryogenic arrays	High (0.90–0.98)
Type IV: Optomechanical	Resonators	Force, acceleration	MEMS arrays	Medium (0.75–0.90)

Table 1.11: Taxonomy of QFI systems with reconstruction fidelity potential.

This book focuses on **Type I (NV centers)** as the exemplar platform, but the QFI framework—particularly the operator stack and Q_{IFOM} formalism—generalizes to all types.

1.9.1 Why NV Centers Are the Exemplar Platform

NV centers in diamond uniquely enable QFI because:

1. **Multi-physics capability**: Single defect senses B, T, strain, E-field through different Hamiltonian terms
2. **Room temperature operation**: No cryogenics required, enabling integration with probe stations
3. **Optical readout**: Naturally compatible with wide-field imaging using camera-based detection
4. **Well-characterized forward models**: Biot-Savart, thermal diffusion are textbook physics

5. **Dense arrays achievable**: 10^{10}–10^{12} NV/cm^3 enable high sensitivity
6. **Non-destructive**: No sample contact or damage during measurement

Physical Quantity	**NV Sensitivity**	**Forward Model $\mathcal{G}$**	**Chapter**
Magnetic field **B**	~ 1 nT/$\sqrt{\text{Hz}}$	Biot-Savart law	Ch. 10
Temperature T	~ 10 mK/$\sqrt{\text{Hz}}$	Thermal diffusion	Ch. 11
Strain ε	$\sim 10^{-6}/\sqrt{\text{Hz}}$	Elasticity theory	Ch. 11
Electric field **E**	~ 200 V/cm/$\sqrt{\text{Hz}}$	Stark shift	Ch. 11

Table 1.12: NV center multi-physics sensing capabilities with associated forward models and book chapter references.

1.10 Worked Examples

Example 1.10.1 (Complete QFOM and QIFOM Calculation for TSV Inspection)**. Problem**: A QFI system for through-silicon via (TSV) inspection has:

- Quantum sensitivity: $\eta_q = 1$ µT/$\sqrt{\text{Hz}}$
- Classical alternative sensitivity: $\eta_{\text{classical}} = 1$ mT/$\sqrt{\text{Hz}}$
- Parallel channels: $N_{\text{parallel}} = 512 \times 512 = 262,144$
- Acquisition time: $t_{\text{acquisition}} = 1$ s
- Multi-physics factor: $\Phi_{\text{multi}} = 3$ (B + T + strain)
- Reconstruction fidelity: $\Gamma_{\text{inv}} = 0.85$
- Model-mismatch penalty: $\Gamma_{\text{mm}} = 0.90$

Calculate Q_{FOM} and Q_{IFOM}, and interpret the results.
Solution:
Step 1: Calculate QFOM (measurement throughput)

$$Q_{\text{FOM}} = \frac{\eta_q}{\eta_{\text{classical}}} \times \frac{N_{\text{parallel}}}{t_{\text{acquisition}}} \times \Phi_{\text{multi}} \tag{1.19}$$

$$= \frac{1 \text{ µT}/\sqrt{\text{Hz}}}{1 \text{ mT}/\sqrt{\text{Hz}}} \times \frac{262,144}{1 \text{ s}} \times 3 \tag{1.20}$$

$$= 1000 \times 262,144 \times 3 \tag{1.21}$$

$$= 7.86 \times 10^8 \text{ s}^{-1} \tag{1.22}$$

Step 2: Calculate QIFOM (imaging figure of merit)

$$Q_{\text{IFOM}} = Q_{\text{FOM}} \times \Gamma_{\text{inv}} \times \Gamma_{\text{mm}} \tag{1.23}$$

$$= 7.86 \times 10^8 \times 0.85 \times 0.90 \tag{1.24}$$

$$= 6.01 \times 10^8 \text{ s}^{-1} \tag{1.25}$$

Interpretation:

- The $Q_{\text{FOM}} = 7.86 \times 10^8$ represents measurement throughput equivalent to ∼800 million single-point classical measurements per second.

- The $Q_{\text{IFOM}} = 6.01 \times 10^8$ is 23% lower, reflecting reconstruction limitations ($\Gamma_{\text{inv}} \times \Gamma_{\text{mm}} = 0.765$).
- Both metrics indicate exceptional performance; however, only Q_{IFOM} captures the true imaging capability.
- The $\Gamma_{\text{inv}} = 0.85$ suggests room for improvement through better regularization or additional physics channels.

Example 1.10.2 (From Field Map to Current Reconstruction: QFM vs QFI)**. Problem**: Demonstrate the conceptual difference between QFM and QFI outputs for the same measurement data.

Given: A system measures magnetic field $B_z(x, y)$ with 512×512 pixels, standoff $d = 5$ µm, noise $\sigma_B = 0.1$ µT.

QFM Output (Measurement Only):

- Calibrated field map: $B_z(x, y) \pm \sigma_B$
- Deliverable: "The magnetic field at pixel (i, j) is 1.2 ± 0.1 µT"
- No source inference; interpretation left to user

QFI Output (Complete Imaging):
Apply reconstruction operator $\mathcal{R}$ to invert the Biot-Savart forward model:

$$\hat{\mathbf{J}}(\mathbf{r}) = \mathcal{R}\{B_z(x, y)\} \tag{1.26}$$

Deliverables:

1. **Source estimate**: 3D current density map $\hat{\mathbf{J}}(x, y, z)$
2. **Uncertainty**: $\sigma_J(\mathbf{r})$ from Fisher Information
3. **Reconstruction residual**: $\|B_{\text{measured}} - \mathcal{G}\{\hat{J}\}\|$
4. **Statement**: "There is a 50 ± 5 µA current at depth 8 ± 1 µm with 95% confidence"

Key Insight: QFM tells you *what the field is*; QFI tells you *what caused it*.

1.11 Chapter Summary

1.11.1 Key Concepts Introduced

1. **Two-layer taxonomy**: QFM (field measurement) produces $F(\mathbf{r})$; QFI (source reconstruction) produces $\hat{S}(\mathbf{r}) \pm \sigma_S$
2. **Operator stack**: The complete imaging pipeline $S \xrightarrow{\mathcal{G}} F \xrightarrow{\mathcal{M}} D \xrightarrow{\mathcal{R}} \hat{S}$
3. **QFI Gate criterion**: System is QFI only if it delivers source estimate, uncertainty, residual, and validation
4. **QFOM**: Measurement throughput metric (s^{-1})
5. **QIFOM**: Complete imaging FOM including reconstruction fidelity: $Q_{\text{IFOM}} = Q_{\text{FOM}} \times \Gamma_{\text{inv}} \times \Gamma_{\text{mm}}$
6. Γ_{inv}: Reconstruction fidelity factor measuring CRB efficiency

7. Γ_{mm}: Model-mismatch penalty from calibration errors
8. Φ_{multi}: Multi-physics correlation factor (≥ 1)
9. **Historical parallel**: CCD revolution as template for QFI paradigm shift
10. **NV centers**: Exemplar platform enabling multi-physics QFI at room temperature

1.11.2 Design Rules from This Chapter

Rule	Statement
DR 1.1	QFI requires all four operators: forward model $\mathcal{G}$, measurement $\mathcal{M}$, reconstruction $\mathcal{R}$, and uncertainty quantification
DR 1.2	Target the weakest factor for optimization (multiplicative improvement principle)
DR 1.3	SNR scales as $\sqrt{t}$; parallelism is more efficient than integration time for throughput
DR 1.4	Multi-physics improves both Φ_{multi} (information) AND Γ_{inv} (conditioning)

Table 1.13: Design rules summary for Chapter 1.

1.11.3 Equations to Remember

Equation	Name	Reference
$S \xrightarrow{\mathcal{G}} F \xrightarrow{\mathcal{M}} D \xrightarrow{\mathcal{R}} \hat{S}$	Operator Stack	Eq. (1.1)
$Q_{\text{FOM}} = \frac{\eta_q}{\eta_{\text{classical}}} \times \frac{N_{\text{parallel}}}{t_{\text{acquisition}}} \times \Phi_{\text{multi}}$	QFM Figure of Merit	Eq. (1.2)
$Q_{\text{IFOM}} = Q_{\text{FOM}} \times \Gamma_{\text{inv}} \times \Gamma_{\text{mm}}$	QFI Imaging FOM	Eq. (1.3)

Table 1.14: Key equations from Chapter 1.

Problems and Solution Hints

Problem 1.1: QFM vs QFI Classification

A research group claims to have built a "quantum field imager" that measures magnetic fields using a 256×256 NV array. They report field maps with 100 nT resolution but do not perform any source reconstruction.

(a) Is this system QFM or QFI? Justify using Definition 1.2.1 and 1.2.2.

(b) What additional components (operators) would be needed to qualify as QFI per the QFI Gate criterion?

(c) Estimate reasonable values for Γ_{inv} if they were to add reconstruction, assuming their forward model is Biot-Savart with $\kappa \sim 500$.

Hint: Apply the QFI Gate criterion systematically. For (c), use Eq. (1.18).

Problem 1.2: QIFOM Optimization Strategy

A QFI system has the following parameters:

- $\eta_q/\eta_{\text{classical}} = 500$
- $N_{\text{parallel}} = 10^5$
- $t_{\text{acquisition}} = 2$ s
- $\Phi_{\text{multi}} = 2$
- $\Gamma_{\text{inv}} = 0.60$ (poorly conditioned inverse problem)
- $\Gamma_{\text{mm}} = 0.95$

(a) Calculate the current Q_{FOM} and Q_{IFOM}.

(b) Which single factor improvement would have the largest impact on Q_{IFOM}? Justify quantitatively.

(c) If Γ_{inv} could be improved to 0.90 by adding a third physics channel (which also increases Φ_{multi} to 3), calculate the new Q_{IFOM} and the total improvement factor.

Hint: Compare the improvement ratios for each factor.

Problem 1.3: Depth-Amplitude Ambiguity

A buried current at depth z produces magnetic field $B \propto I/z^2$ and thermal signature $T \propto I^2 R$ that diffuses with characteristic width $\sigma_T \propto \sqrt{D \cdot z}$.

(a) Show mathematically why single-physics (magnetic only) measurement cannot uniquely determine both current magnitude I and depth z.

(b) Derive how adding thermal measurement breaks this degeneracy.

(c) Estimate Φ_{multi} for this two-physics configuration.

Hint: Set up the Fisher Information matrix for parameters (I, z) and examine its rank for single vs. multi-physics cases.

Problem 1.4: Condition Number and Γ_{inv}

For a discrete forward model $\mathbf{F} = \mathbf{GS} + \mathbf{n}$ where $\mathbf{n}$ is Gaussian noise with variance σ^2:

(a) Write the least-squares reconstruction $\hat{\mathbf{S}} = (\mathbf{G}^T\mathbf{G})^{-1}\mathbf{G}^T\mathbf{F}$.

(b) Using the SVD $\mathbf{G} = \mathbf{U}\mathbf{\Sigma}\mathbf{V}^T$, show that the reconstruction variance scales with κ^2 where $\kappa = \sigma_{\max}/\sigma_{\min}$.

(c) Propose Tikhonov regularization and analyze its effect on Γ_{inv}.

Hint: The condition number determines how noise amplifies through inversion.

Problem 1.5: CCD Revolution Analysis (Literature Research)

Research the historical transition from PMT photometry to CCD imaging in astronomy (1980s–1990s).

(a) Identify three specific scientific discoveries that were enabled by CCD imaging but would have been impossible with PMT photometry.

(b) For each discovery, explain whether it required only higher throughput (QFM-equivalent) or true imaging capability (QFI-equivalent).

(c) Draw explicit parallels to potential QFI-enabled discoveries in semiconductor metrology.

Hint: Consider dark energy discovery (Type Ia supernovae), gravitational lensing surveys, and exoplanet transit photometry.

References

[1.1] Degen, C. L., Reinhard, F., & Cappellaro, P. (2017). Quantum sensing. *Reviews of Modern Physics*, 89(3), 035002.

[1.2] Taylor, J. M., et al. (2008). High-sensitivity diamond magnetometer with nanoscale resolution. *Nature Physics*, 4(10), 810–816.

[1.3] Janesick, J. R. (2001). *Scientific Charge-Coupled Devices*. SPIE Press.

[1.4] Glenn, D. R., et al. (2017). High-resolution magnetic resonance spectroscopy using a solid-state spin sensor. *Nature*, 555(7696), 351–354.

[1.5] Nowodzinski, A., et al. (2015). Nitrogen-vacancy centers in diamond for current imaging at the redistributive layer level of integrated circuits. *Microelectronics Reliability*, 55(9–10), 1549–1553.

[1.6] Kehayias, P., et al. (2022). Imaging electric current in ICs using NV-diamond. *Physical Review Applied*, 17(1), 014022.

[1.7] Barry, J. F., et al. (2020). Sensitivity optimization for NV-diamond magnetometry. *Reviews of Modern Physics*, 92(1), 015004.

[1.8] Levine, E. V., et al. (2019). Principles and techniques of the quantum diamond microscope. *Nanophotonics*, 8(11), 1945–1973.

[1.9] Tetienne, J.-P., et al. (2017). Quantum imaging of current flow in graphene. *Science Advances*, 3(4), e1602429.

[1.10] Kay, S. M. (1993). *Fundamentals of Statistical Signal Processing: Estimation Theory*. Prentice Hall.

[1.11] Li, Y., et al. (2022). Wide-field circuit tomography using nitrogen-vacancy centers in diamond. *Optics Express*, 30(17), 30495–30508.

[1.12] Broadway, D. A., et al. (2020). Improved current density and magnetization reconstruction through vector magnetic field measurements. *Physical Review Applied*, 14(2), 024076.